

Journal of Materials Chemistry C

Accepted Manuscript



This is an *Accepted Manuscript*, which has been through the Royal Society of Chemistry peer review process and has been accepted for publication.

Accepted Manuscripts are published online shortly after acceptance, before technical editing, formatting and proof reading. Using this free service, authors can make their results available to the community, in citable form, before we publish the edited article. We will replace this *Accepted Manuscript* with the edited and formatted *Advance Article* as soon as it is available.

You can find more information about *Accepted Manuscripts* in the [Information for Authors](#).

Please note that technical editing may introduce minor changes to the text and/or graphics, which may alter content. The journal's standard [Terms & Conditions](#) and the [Ethical guidelines](#) still apply. In no event shall the Royal Society of Chemistry be held responsible for any errors or omissions in this *Accepted Manuscript* or any consequences arising from the use of any information it contains.



Journal Name

ARTICLE

Effect of single atom substitution in Benzochalcogenadiazole Acceptors on the performance of ternary Memory Devices

Zhaojun Liu,^a Jinghui He,^b Hao Zhuang,^b Hua Li,^{b*} Najun Li,^b Dongyun Chen,^b Qingfeng Xu,^b Jianmei Lu,^{*bc} Keqin Zhang,^a and Lihua Wang^b

Received 00th January 20xx,
Accepted 00th January 20xx

DOI: 10.1039/x0xx00000x

www.rsc.org/

Herein, three conjugated organic molecules comprised of diethylamine donor, pyrimidine and benzochalcogenodiazole acceptors (where the chalcogen atom are varied from O, S to Se), named as PBOP, PBTP, and PBSeP, were synthesized and fabricated into resistive random access memory devices. Structural analysis and theoretical calculations show that the three molecules have almost the same crystal structures and orientations in film state but different backbone planarities, electron affinities, intra- and intermolecular interactions, which tune the molecular packing and optical absorption. All the compounds exhibited non-volatile ternary memory characteristics while PBOP showed the lowest switching threshold voltages (1.2 V) and highest I_{on}/I_{off} ratios (10^5 and 10^3).

Introduction

Organic conjugated materials, especially small molecules, have attracted extensive attention in recent years since their potential applications in the fields of solar cells,¹ field effect transistors,² sensors³ and memories^{4,5} owing to their low cost, flexibility and tunability through structural design.⁶ For example, as one promising kind of application of organic materials, resistive random access memory (RRAM) received considerable attention because of the capability of layer-by-layer stacking and/or multilevel information storage and multilevel RRAMs have been achieved by rationally designing of molecular structure.^{4,5} Generally, incorporation of heterocyclic units with electron donating (donors) and withdrawing (acceptor) group into molecule backbones can greatly improve the conjugation and tune the performance of organic electronic devices.⁷ To explore structure–property relationships of organic memory devices, researchers varied types, positions, numbers and ratios⁸ of the donor and acceptors⁹ of the active organic molecule and investigated their effects on the device performances. However, in such cases, the molecular structure changes too much and induces complexity to correctly correlate the microscopic structural effect to macroscopic device phenomena. In this context, the choice of a series of “infinitesimal” variations of the molecules—substitution of a single atom of particular donor/acceptors in the molecule appear to be more elegant and

desirable, but scarcely reported.^{10,11b,11c} One category of heterocycles, benzochalcogenadiazoles including benzoaxadiazole (BO), benzothiadiazole (BT), benzoselenadiazole (BSe), are typical examples of single atom substitution and intensively employed as conjugative building blocks for improving device performance.¹¹ Organic materials containing BT show relatively higher electron mobilities and I_{on}/I_{off} ratios in devices due to its stronger electron withdrawing ability and more intrinsic S...N interactions between the thiadiazole rings.¹² BSe can effectively tune the polarizability, optical and electronic properties of organic conjugated chain.¹³ BO was not widely studied but several studies examining molecular backbones show that BO is a stronger acceptor than BT and BSe due to the larger electron affinity of oxygen.¹⁴ In addition, BO's ability to form coplanar and quinoid structures enhance the air stability of as-fabricated devices.¹⁵

Nevertheless, their effects on device performances are reported to be contradictory. It was also reported recently that BO/BSe as building blocks can guarantee stronger polarity, atomic interaction and electron affinity of the target molecules than BT.^{15,16} The obtained BO/BSe-based devices show the higher redox stability, higher I_{on}/I_{off} ratio, longer cycle life, lower bandgap and lower operation voltage than that of BT.^{11a,17} More confusingly, when BO and BSe is located in electron-donating building block, the optoelectronic performance of devices are only slightly improved or even decreased.^{11c,18} Herein, the questions remain on how and why those organic electronic devices were tuned so significantly by these three benzochalcogenadiazoles. Any study toward this question will be useful for device optimizations through structural design of new organic materials.

In this report, we synthesized three benzochalcogenadiazoles derivatives where the chalcogen of the benzodiazole moiety is systematically varied from oxygen to sulfur to selenium (**Figure 1**). The RRAMs devices based on these molecules were fabricated and investigated. The results of experimental measurements and

^a College of Textile and Clothing Engineering, Soochow University, Suzhou 215123, China

^b College of Chemistry, Chemical Engineering and Materials Science, Collaborative Innovation Center of Suzhou Nano Science and Technology, Soochow University, Suzhou 215123, P. R. China. E-mail: lujm@suda.edu.cn; Fax: +86 512 65880367; Tel: +86 512 65880368 China

^c State Key Laboratory of Treatments and Recycling for Organic Effluents by Adsorption in Petroleum and Chemical Industry, Suzhou 215123, P. R.

[†] Electronic supplementary information (ESI) available: Experimental procedures, The compositions of the small molecules, TGA, memory device stability, SEM images, DFT molecular simulation results. See DOI: 10.1039/b000000x/.

theoretical simulations surprisingly demonstrated exotic trends of the device performances, different from previous research results.

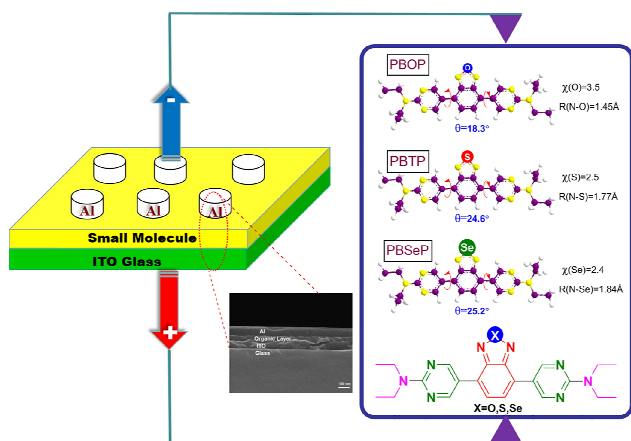


Figure 1. From left to right, Schematic diagram of sandwich device. SEM image of a cross-section view of the device. Chemical structures, optimized geometries, electronegativity of the heteroatom, bond length of N-X, and dihedral angles between the planes of the two pyrimidine rings adjacent to the central benzodiazole unit.

Experimental section

Materials

5-bromo-2-iodopyrimidine, benzothiadiazole, benzofuroxan, sodium borohydride, [1,1-Bis(diphenylphosphino)ferrocene] dichloropalladium(II), bis(pinacolato)diboron, (β-4)-platinum were purchased from commercial suppliers (TCI, Alfa Aesar, Sigma-Aldrich) and used without further purification. Solvents used were dried and distilled by standard methods prior to use. All reactions were carried out under air atmosphere unless stated. The following compounds were synthesized according to the procedures reported in the literature (see ESI[†] for details): 5,5'-(benzo[c][1,2,5]oxadiazole-4,7-diyl)bis(N,N-diethylpyrimidin-2-amine), 5,5'-(benzo[c][1,2,5]thiadiazole-4,7-diyl)bis(N,N-diethyl pyrimidin-2-amine), 5,5'-(benzo[c][1,2,5]selenadiazole-4,7-diyl) bis(N,N-diethylpyrimidin-2-amine).

Preparation of PBOP, PBTP and PBSeP

Synthesis of compound PBOP (5,5'-(benzo[c][1,2,5] oxadi azole-4,7-diyl)bis(N,N-diethylpyrimidin-2 -amine). A mixture of 4, 7-dibromo-2, 1, 3-benzooxadiazole (1.38 g, 5 mmol), compound 2 (2.25 g, 15 mmol), potassium carbonate (2.76 g, 20 mmol), Pd(PPh₃)₄ (47 mg, 0.04 mmol), H₂O (20 mL) and toluene (30 mL) was heated at 90 °C for 10 h. After cooling, the mixture was poured into water and extracted with dichloromethane. The organic layer was washed with water and then dried with anhydrous Na₂SO₄. After the solvent was evaporated, the crude product was recrystallized from ethanol to afford **PBOP** (1.29 g, 62%) as a crimson solid. ¹H NMR (400 MHz, CDCl₃) δ = 9.01 (s, 4H), 7.51 (s, 2H), 3.72 (dd, J = 13.9, 6.9 Hz, 8H), 1.26 (t, J = 6.9 Hz, 12H). ¹³C NMR (101 MHz,

CDCl₃) δ = 160.53, 156.89, 148.80, 125.35, 123.08, 116.61, 42.25, 13.07. HRMS: Anal. Calcd. For C₂₂H₂₆N₈O [M + H]⁺ 419.2230 found 419.2241.

Compounds PBTP and PBSeP were synthesized use using a similar procedure for compound PBOP.

Synthesis of compound PBTP (5,5'-(benzo[c][1,2,5]thiadi azole-4,7-diyl)bis(N,N-diethyl pyrimidin-2-amine)). 1.63 g, 75%, crimson solid. ¹H NMR (400 MHz, CDCl₃) δ = 8.98 (s, 4H), 7.67 (s, 2H), 3.70 (dd, J = 13.3, 6.5 Hz, 8H), 1.24 (t, J = 6.7 Hz, 12H). ¹³C NMR (101 MHz, CDCl₃) δ = 160.28, 157.55, 153.75, 127.70, 125.53, 118.41, 42.14, 13.09. HRMS: Anal. Calcd. For C₂₂H₂₆N₈S [M + H]⁺ 435.2001 found 435.2011.

Synthesis of compound PBSeP (5,5'-(benzo[c][1,2,5]selenadi azole-4,7-diyl)bis(N,Ndiethyl pyrimidin-2-amine)). 2.00 g, 83%, orange solid. ¹H NMR (400 MHz, CDCl₃) δ = 8.88 (s, 4H), 7.50 (s, 2H), 3.73 (dd, J = 13.5, 6.6 Hz, 8H), 1.27 (t, J = 6.9 Hz, 12H). ¹³C NMR (101 MHz, CDCl₃) δ = 160.25, 159.47, 157.81, 129.55, 126.04, 119.01, 42.13, 13.10. HRMS: Anal. Calcd. For C₂₂H₂₆N₈Se [M + H]⁺ 483.1446 found 482.1452.

Fabrication of the Memory Device

The indium-tin-oxide (ITO) glass was pre-cleaned by ultra-sonication in solvent by sequence for 10 min, inclusive of water, acetone and alcohol. The organic film was prepared on glass slides from the 1,2-dichlorobenzene solution at room temperature by spin coating. The film thickness was about 80 nm determined by a quartz oscillator. A layer of Al, about 100 nm in thickness was thermally evaporated and deposited onto the organic surface at a pressure of about 5 × 10⁻⁶ Torr through a shadow mask to form the top electrode of 0.0314 mm² in area. In addition, the 5 nm thick LiF layer was evaporated under high vacuum before the evaporation of Al when necessary.

Measurement

All measurements of the devices were conducted under ambient conditions, without any encapsulation, using an HP 4145B semiconductor parameter analyzer equipped with HP 8110A pulse generator. NMR spectra were collected by an Inova 400 MHz FT-NMR spectrometer. High resolution mass spectra (HRMS) were obtained using MicroMass TOF-MS spectrometer (EI). UV-vis absorption spectra were carried out at room temperature from 250 to 750 nm with a Shimidazu UV-3600 spectrophotometer. Thermo gravimetric analysis (TGA) was conducted on a TA instrument Dynamic TGA 2950 at an annealing rate of 10 °C·min⁻¹ under a nitrogen flow rate of 50 mL min⁻¹. SEM images were taken on a Hitachi S-4700 scanning electron microscope. Atomic force microscopy (AFM) measurements were performed by using a MFP-3D-TM (Digital Instruments/Asylum Research) AFM instrument in tapping mode. X-ray diffraction (XRD) patterns were taken on an X'Pert-Pro MPD X-ray diffractometer. 2D GISAXS measurement was carried out on Anton Paar SAXS pace Analyzer.

Results and Discussion

Synthesis and Characterization

The structures and the synthetic methods for the synthesis of three molecules are presented in **Figure S1**. Molecule 1 (M1), M2, M3, M4, M5, M6, and M7 were prepared as described elsewhere.¹⁹ From Suzuki-Miyaura couplings of M3, M5, and M7 with M2 in the presence of Pd[P(C₆H₅)₃]₄ as the catalyst and K₂CO₃ as the base in Toluene/H₂O at 90°C for 12 h, we obtained the compounds PBOP, PBTP and PBSeP in yields of

62–83%, respectively. The chemical structures of the moieties and the molecules were verified by ¹H NMR, ¹³C NMR and HRMS spectroscopy. More details are described in the Supporting Information. Thermal stability of the molecules was investigated with thermogravimetric analysis as shown in **Figure S2** and Table 1. The TGA analysis reveals that the temperatures (Td) to lose 5% weight of PBOP, PBTP, and PBSeP were 192.5, 282.2, and 280.7 °C, respectively. Therefore the thermal stabilities of three molecules are adequate for their applications in memory as well as other optoelectronic devices.

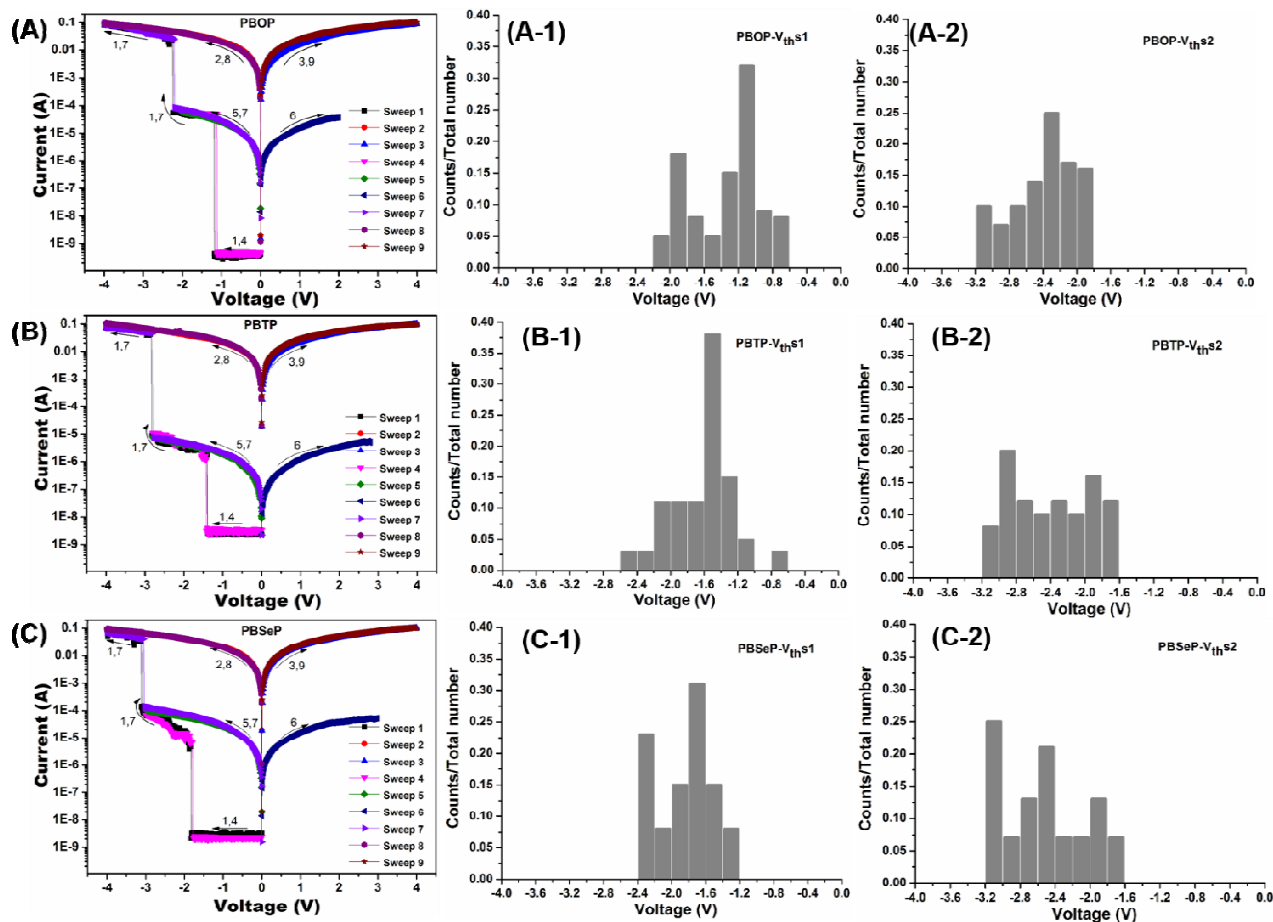


Figure 2. Typical I–V curves of the (A) ITO/PBOP or (B) PBTP or (C) PBSeP/Al memory device; A,B,C-1) the statistical data of reproducibility and ON1 state switching threshold voltages distribution, (A,B,C-2) ON2 state switching threshold voltages distribution.

Current–voltage (I–V) Characteristics

The memory devices based on PBOP, PBTP and PBSeP were fabricated as ITO/small-molecule/Al sandwiched devices and the current–voltage (I–V) characteristics of these devices are shown in **Figure 2**. In the first sweep from 0 to –4 V (sweep 1), the compound PBOP based devices display two sharp transitions from a low conductive (OFF, “0”) state to an intermediately conductive (ON1, “1”) state, finally to a high conductive (ON2, “2”) state at voltages (V_{th}) of –1.2 and –2.3 V. The OFF to-ON1 and -ON1 to -ON2 transitions can be regarded as a “writing” operation for the memory device. As shown by Sweep 2, it remains in the ON2 state

when the negative sweep was repeated or followed by a reversed scanning (sweep 3). Therefore, this device exhibits typical ternary memory behaviour.

Another cell of the device was measured over a voltage range of 0 to –2 V (sweep 4) and showed the first onset V_{th} s at –1.1 V, which suggests switching from “OFF” to “ON1”. Subsequent forward and reverse scans from 0 to –2 V (sweep 5 and 6) indicate that this device remains in its ON1 state, even when the external voltage was removed. A following sweep 7 from 0 to –4 V convert the ON1 to ON2 state at the –2.2 V. Again, the ON2 state could survive from following negative and positive sweeps of a large voltage (Sweeps 8 and 9). The above three states distinguish themselves by a current

ratio of $1:10^5:10^8$ for "OFF", "ON1", and "ON2" states. In short, ternary WORM (write-once-read-many-times) memory behaviour was achieved in our experiments.

Similarly, the other two molecules, PBTP and PBSeP based devices were sequentially investigated and both show ternary WORM characteristics. PBTP based devices are of switching threshold voltages ($V_{th,s}$) at -1.4 V and -2.8 V, while -1.8 V and -3.1 V are found for that of PBSeP (Figure 2 B-1, C-1). One should be noted that the threshold voltages of PBOP are markedly lower than that of PBTP and PBSeP. Moreover, the conductance of PBOP-device at OFF state is obviously lower than that of PBTP and PBSeP, which indicates that PBOP-devices may be more favorable for potential application because of its lower online power consumption and lower operation voltages.

In order to rule out the possible metal filaments phenomenon happened in above devices, we deposited a layer of LiF (5 nm) between the film and aluminium electrode to prevent aluminium nanoparticles penetrating into the functional film. Herein, the formed devices all exhibit original WORM behaviour as shown in Figure S6, which indicated that the observed WORM behaviour is irrelevant to the metal filament.

Considering the reproducibility of the switching phenomenon is an important parameter for memory devices, we count on 50 cells to investigate the cell-to-cell uniformity for the three molecules based devices. The statistical data shows that the thresholds voltages of ON1 have narrower distribution than that of ON2 (Figure 2), which indicates that the ON1 states of the fabricated devices compared to ON2 are more stable. Regarding the stability, it is noteworthy that all the storage states of the memory devices of PBOP, PBTP and PBSeP are highly stable for more than one million (10^6) continuous read pulses at -1 V without any significant degradation (see Figures. S3a, b and c). In addition, the currents of all the states in the three devices are stable under a constant voltage stress of -1 V for up to 10 hours (see Figure. S3 A, B and C).

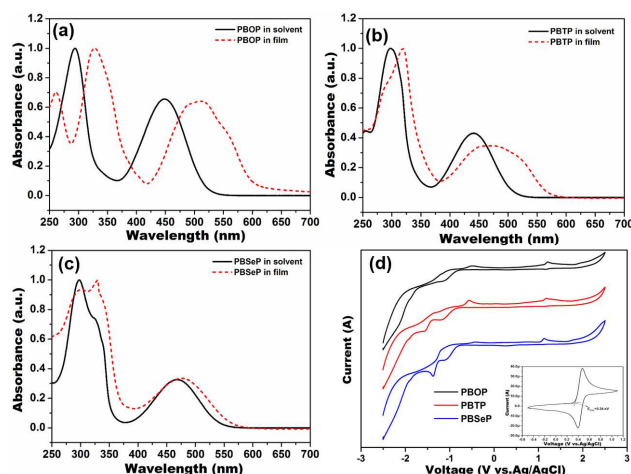


Figure 3. a, b, c) UV-Visible absorption spectra of the three compounds in CH_2Cl_2 solution and film. d) Cyclic voltammetry (CV) curves of the three compounds on the ITO electrode in $0.1\text{M Bu}_4\text{NPF}_6/\text{CH}_3\text{CN}$ solution with Ag/AgCl as the reference electrode and Pt wire as the counter electrode. The scan rate was 100 mV s^{-1} . The inset shows the CV curve of ferrocene, swept in the same conditions as for the three

small molecules ($E_{1/2}(\text{ferrocene})$ was measured to be 0.34 V vs. Ag/AgCl in CH_3CN).

Optical and Electrochemical Properties

The UV-vis spectra of all compounds in dichloromethane solution and film state are investigated to reveal the molecular electronic properties and the stacking manner in the film (Figure 3 and in Table 1). The absorption spectra of three molecules showed dual-band absorption: the higher energy bands (~ 300 nm) due to conjugation and the lower energy bands ($\sim 450\text{nm}$) from intramolecular charge transfer.²¹ It's worth noting that, some interesting trends are observed in these spectra. First, the λ_{max} values of both peaks exhibit red shift when heavier chalcogens are substituted into the benzodiazole unit. This could be attributed to the increasing electron density and atomic radius of the heteroatom (from O to Se) and resulting in an improved intramolecular charge transfer (ICT). Second, the absorption bands are broader in the film than in solution, indicating improved planarity of the molecular backbone and enhanced intermolecular interactions in film state. Third, the absorption coefficient of the low-energy band decreases in intensity while the high-energy band remains constant upon moving from O to S to Se, which can be ascribed to the loss of electronegativity of the heteroatom and the acceptor unit's ability to produce and stabilize a charge-separated state.⁸ Fourth, energy gap variation trend from solution UV and electrochemical spectra are the same with $\text{PBSeP} < \text{PBOP} < \text{PBTP}$ whereas the film gaps has a different sequence of $\text{PBOP} < \text{PBTP} < \text{PBSeP}$. Since both solution UV and electrochemical spectra represent the electronic properties of individual molecules, the varied sequence of energy gaps of the films in fact reflect that the stacking and crystallinity play an crucial role to determine the ensemble of molecules. The maximum absorption peaks of PBOP, PBTP, and PBSeP in the films show redshift of 65.5 nm, 34.3 nm and 12.2 nm, respectively compared to their solution spectra which indicate considerable intermolecular interaction and ordered molecular stacking in the solid state. The lowest band gap and the largest red-shift of PBOP than PBTP and PBSeP suggest the more planar configuration between the pyrimidine ring and BO moiety in PBOP, which we will discuss later.

The electrochemical properties of the three molecules films on an indium-tin oxide (ITO) glass substrate were studied through cyclic voltammetry (CV) in anhydrous acetonitrile. In Figure 3d, the onset oxidation (reduction) potentials of compounds PBOP, PBTP and PBSeP are 1.13 (-1.10) eV, 1.12 (-1.14) eV, 1.07 (-1.08) eV, respectively. On the basis of these values, we estimated the HOMO and LUMO energy levels according to the energy level of the ferrocene reference (4.8 eV below vacuum level) by the following equation:¹²

$$E_{\text{HOMO}} = -(E_{\text{onset}}^{\text{ox}} + 4.8 - E_{\text{Ferrocene}}) \quad (1)$$
$$E_{\text{LUMO}} = -(E_{\text{onset}}^{\text{red}} + 4.8 - E_{\text{Ferrocene}}) \quad (2)$$

As shown in Table 1 the HOMO energy levels of PBOP, PBTP and PBSeP are -5.59 , -5.58 and -5.53 eV, respectively. The low HOMO levels suggest that all compounds would be stable against oxidation in air. The LUMO energy levels of PBOP, PBTP and PBSeP are -3.36 , -3.32 and -3.38 eV, respectively. Thus, by

replacing O atoms with S atoms or Se atoms, the degree of electron-deficient characteristic of benzoxadiazole unit decreases, resulting in stabilization of the HOMO, destabilization of the LUMO. Moreover, all molecules show poor reversibility of the reduction processes, which indicates

limited charge transport in the thin-film state. Above all, the photoelectric properties of the conjugated compounds can be easily tuned by simply incorporating different electron-deficient atoms.

Table 1. Optical and electrochemical properties of the three synthesized molecular films

Index	^a λ_{onset} (nm)	^a E_g^{optical} (eV)	^b λ_{onset} (nm)	^b E_g^{optical} (eV)	^c $E_{\text{onset}}^{\text{red}}$ (eV)	^b $E_{\text{onset}}^{\text{ox}}$ (eV)	^d HOMO (eV)	^d LUMO (eV)	^e $E_g^{\text{electrical}}$ (eV)	$\Phi_{\text{ITO}}-E_{\text{HOMO}}$ (eV)	$E_{\text{LUMO}}-\Phi_{\text{Al}}$ (eV)
PBOP	523.2	2.37	605	2.05	-1.10	1.13	-5.59	-3.36	2.23	0.79	0.94
PBTP	511.4	2.42	570	2.17	-1.14	1.12	-5.58	-3.32	2.28	0.78	0.98
PBSeP	544.3	2.28	560	2.21	-1.08	1.07	-5.53	-3.38	2.15	0.73	0.92

^a The data were calculated by the following equation: bandgap = 1240/ λ_{onset} of the synthesized molecule in CH₂Cl₂. ^b the three synthesized molecular films. ^c Vs Ag/AgCl in acetonitrile. ^d Calculated from cyclic voltammetry. ^e Calculated from the HOMO and LUMO energy level.

X-ray Diffraction and Single crystal structure Analysis

The ordering in the organic thin films was investigated using X-ray diffraction as displayed in **Figure 4a**. The X-ray pattern of PBSeP film is distinct from the above PBOP and PBTP. There are three diffraction peaks for PBOP appeared at 5.86°, 11.78°, and 17.68° and 23.58°, respectively, which have multiple relationships, indicating a highly ordered structure with a d-spacing of 15.1 Å (d_1). According to those reported literatures, it is reasonable to assume that d_1 corresponds to the distance between π -conjugated molecular backbones separated by the alkyl side chain²¹. Similarly, PBTP also has four diffraction peaks in film state: 5.87°, 11.72°, 17.66° and 22.61°, which appear almost at the same positions of PBOP-curves. PBSeP has only a visible feature at 18.82°, with a slightly shrunk d_1 value. These curves indicate that the crystal structure of the grains of two molecules should be the same, despite that their lattice constants are slightly varied. Such a small distortion of the same stacking show the success of our design strategy—change of single atoms of molecules does not cause unwanted

crystal structure variation, rendering the further analysis on structural-properties relationship much more convincing. The X-ray pattern of PBSeP film is distinct from the above two curves.

To further investigate the molecular stacking in the film, we prepared the single crystal of PBSeP and resolve its structure as shown in **Figure 4b**. PBSeP is found to crystallize in a layer-by-layer manner. Visually, its alky side groups condense together by van der waals interaction while its conjugated backbone stacks by π - π interaction. The lattice constant c is 15.0 Å, in agreement with the strongest peak for these films (but not detected by XRD in the case of PBSeP, only (003) was detected to offer a d_1 of 4.95*3=14.9Å). Based on the multiple relationships between these peaks, they could be assigned as (001), (002), (003) and (004), respectively. Single crystals of the other two molecules would offer more structural information but are difficult to prepare thus not reported here.

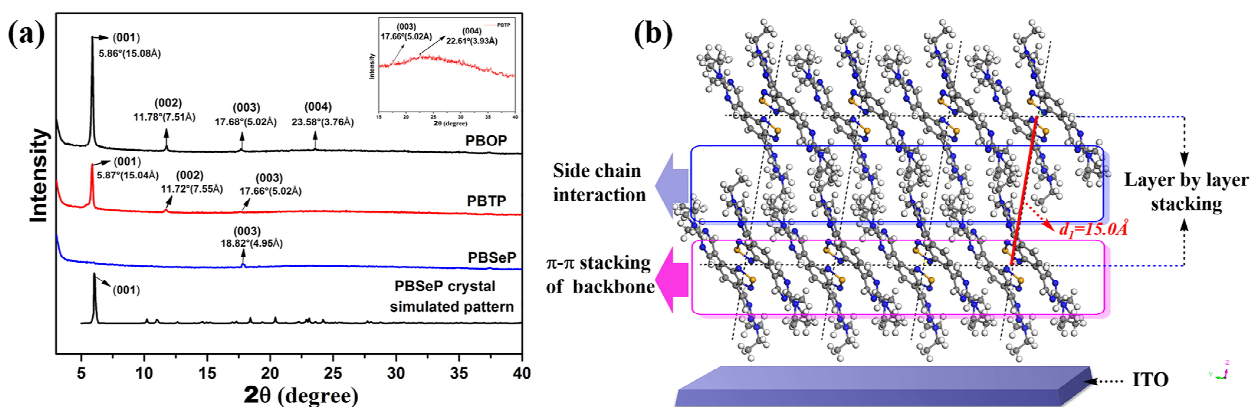


Figure 4. (a) X-ray diffraction patterns of the compounds in solid films. The inset shows amplified features of PBTP curves; (b) Schematic of PBSeP single crystallites in the film stacking orientation. Dashed parallelograms mark the unit cell boundary. The Crystallographic data (excluding structure factors) for the structures reported in this paper have been deposited with the Cambridge Crystallographic Data Centre as deposition No. CCDC 1415038.

In order to further understand the stacking discrepancies, we examined geometric torsions of individual molecules by theoretical calculations. With increasing heteroatom sizes (O < S < Se), the torsions between heteroatom rings and the adjoining pyrimidines

become more acute (18.3° [O] < 24.6° [S] < 25.2° [Se]). Meanwhile, the nitrogen-heteroatom (N-X) bond length increases (Figure 1). On the other hand, experimentally, in the case of PBSeP, the above torsion angle even grows and splits into two: 39.9° and 51.6°, rendering the molecule asymmetric. Comprehensively, the larger

torsion angles and longer N-X bonds result in deterioration of aromaticity and weaken the conjugation among donor and acceptor units. The larger torsion angle will also hinder the closer contact of neighbouring backbone, thus the intermolecular π - π interactions will be attenuated even though the molecular packing keeps unchanged. Thus it is evident that although of the almost the same crystal structure, PBOP is of the best π - π interaction, demonstrating the single atom substitution effect.

Morphology of the thin films

Since the film morphology has a considerable impact on the efficiency of optoelectronic devices,^{18a, 22a} we obtained the topographies of the thin film by atomic force microscopy (AFM).

Figure 5 (a, b, c) displays the surface morphologies of compounds PBOP, PBTP and PBSeP, indicating good film-forming property with root-mean-square (RMS) surface roughness of 2.2, 4.4 and 5.0 nm, respectively. The films of PBOP and PBTP showed the formation of larger grain-like domains (**Figure S4**). PBSeP film exhibited fiber-like domains, which might be produced from molecules aggregation in solution. According to the AFM phase images as shown in **Figure 5(d, e, f)**, we found that compounds PBOP and PBTP displayed homogeneous and continuous films while PBSeP film exhibited partial phase separation. As previously noted, the more severe phase segregation and rougher surface of the PBSeP film presumably arose because of poor solubility and interchain π - π stacking of PBSeP molecule.²³

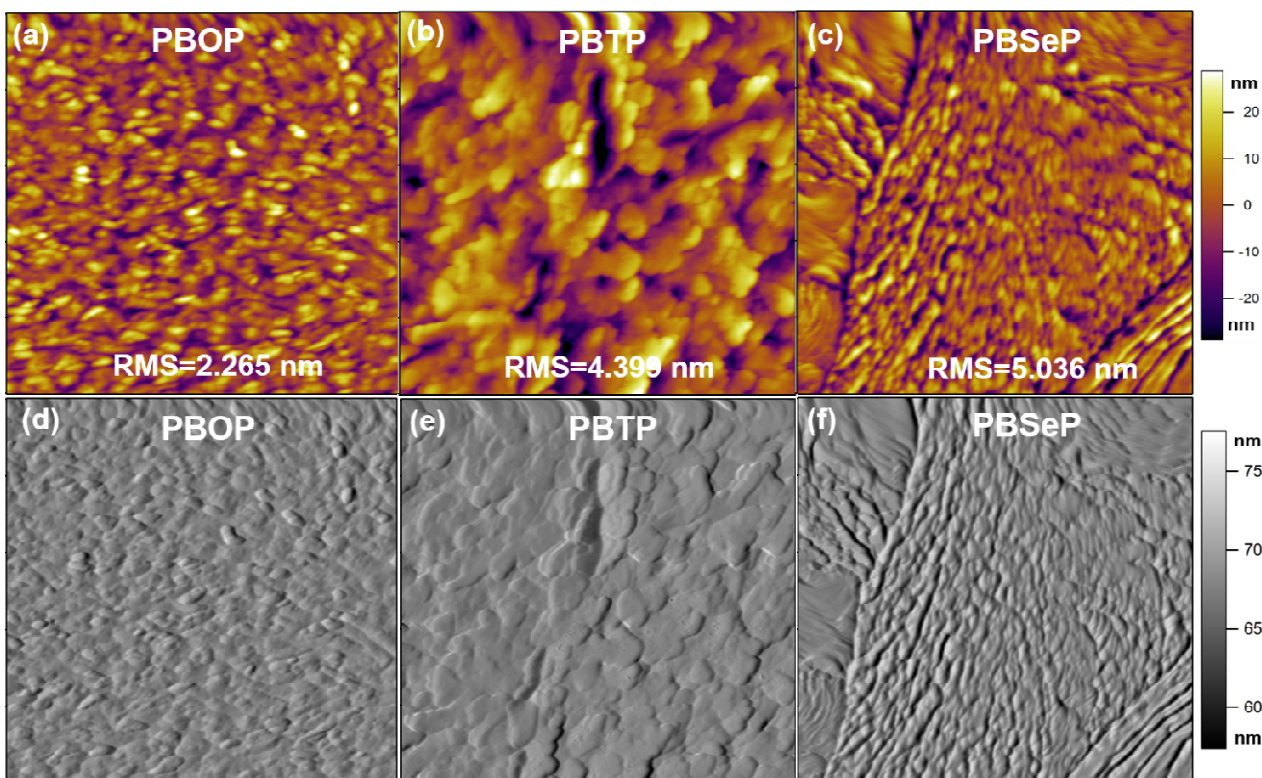


Figure 5. Tapping-mode AFM images ($5\mu\text{m} \times 5\mu\text{m}$): topography image and phase image of the films of PBOP (a, d), PBTP (b, e), and PBSeP (c, f).

Proposed memory mechanisms

To gain insight into the electrical switching behaviour of the memory devices, theoretical calculations have been performed using the density functional theory (DFT) method of B3LYP with the 6-31G (d) basis set. The result shows that the molecular surface has continuous positive molecular electrostatic potential (ESP, in red, **Figure S5**), which can serve as open channels for charge carrier migration throughout the conjugated backbone. The negative ESP regions (in blue) caused by the electron-deficient groups, such as pyrimidine and benzochalcogendiazole segments, can serve as “traps” with different energetic depths to block the motion of charge carriers. **Figure 6a** shows a schematic diagram of the charge transport process in the ternary memory device. Under a low voltage bias, the device is in a low-conductivity (OFF) state

because of the energy barrier between the donor (D) and acceptor-1 (A1), which blocks the electron migration. When the external voltage rises to the first $V_{\text{th,s}}$, the shallow traps from pyrimidine acceptors will be filled, switching the storage cell from OFF to ON1 state. With increasing the applied electric field, the traps arising from the benzochalcogendiazole unit will be filled up sequentially, resulting in the current transition from the ON1 to the ON2 state. The energy levels of the HOMO and LUMO for the memory devices are summarized in **Figure 6b**. The energy barriers between the work function of ITO and HOMO are all lower than the energy barriers between the work functions of Al and LUMO. Thus, holes-migration should dominate the conduction process in three compounds-based devices. Upon undergoing the HOMO to LUMO excitation, intramolecular charge transfer could form a charge-separated state, the trapped electrons are hard to de-trapped

after turning off the power or under reverse voltage, and the formative charge-separated state will not revert to the pristine state and the high-conductivity could be permanently maintained. Therefore, the device exhibits WORM behavior.⁴

Apparently in these systems, oxygen containing heterocycle device shows significantly lower threshold voltages compared the other two. This distinction can be ascribed to the better planarity of benzooxadiazole based molecular backbone, which guarantees a stronger interchain π - π stacking and ordered face-on packing orientation. These advances benefit the formation of free charge transport pathways, making PBOP-based device a promising candidate for high performance QM applications.

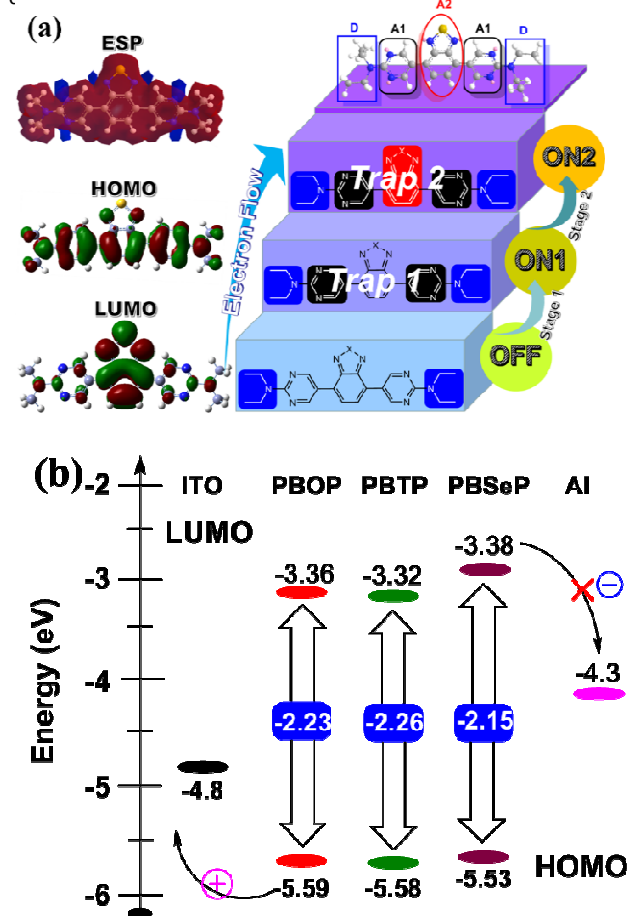


Figure 6. a) HOMO orbital, LUMO orbital, and molecular ESP from DFT calculations. Schematic diagram of the charge carrier transport process in the FKAZO 2-based memory device. b) LUMO and HOMO energy levels for the three molecules, calculation based on CV.

Conclusions

In conclusion, a series of benzochalcogendiazole containing molecules (PBOP, PBTP and PBSeP) have been synthesized and fabricated to memory devices. These compounds stacking in the same crystal structures, thus clearly demonstrating the effect of a single atom substitution on the electrochemical, UV absorption, film morphology, and the molecular packing performance of the system. Among these molecules, the oxygen-containing conjugated backbone allows for increased

planarity and enhanced intermolecular π - π stacking resulting in tighter face-on packing orientation which correlated with good charge transport properties. Therefore, the fabricated PBOP-devices exhibit improved ternary memory performances with the lowest switching threshold voltages and highest I_{on}/I_{off} ratios. These results imply that benzooxadiazole-based compounds can serve as a predominant choice of material for organic multilevel data storage device.

Acknowledgements

This work was financially supported by the Chinese Natural Science Foundation (21176164, 21206102, 21476152 and 21336005), the NSF of Jiangsu Province (BE2013052), Suzhou Nano-project (ZXG2012023) and the Project supported by the Specialized Research Fund for the Doctoral Program of Higher Education of China (Grant no.20113201130003 and 20123201120005) and National Excellent Doctoral Dissertation funds (201455).

Author contributions

Zhaojun Liu synthesized the molecules and was involved in devices measurements. Jinghui He executed the simulation calculations. Jianmei Lu and Hua Li conceived the molecular design and supervised the whole experiments. All authors contributed to the scientific discussion, writing and revision of the manuscript.

Notes and references

- (a) Y. S. Liu, C. C. Chen, Z. R. Hong, J. Gao, Y. Yang, H. P. Zhou, L. T. Dou, G. Li, Y. Yang, *Sci. Rep.* 2013, **3**, 3356. (b) A. K. K. Kyaw, D. H. Wang, D. Wynands, J. Zhang, T. Q. Nguyen, G. C. Bazan, A. J. Heeger, *Nano Lett.* 2013, **13**, 3796. (c) Y. S. Liu, Y. Yang, C. C. Chen, Q. Chen, L. T. Dou, Z. R. Hong, G. Li, Y. Yang, *Adv. Mater.* 2013, **25**, 4657. (d) H. W. Lin, J. H. Chang, W. C. Huang, Y. T. Lin, L. Y. Lin, F. Lin, K. T. Wong, H. F. Wang, R. M. Ho, H. F. Meng, *J. Mater. Chem. A*, 2014, **2**, 3709.
- (a) Y. C. Mei, M. A. Loth, M. Payne, W. M. Zhang, J. Smith, C. S. Day, S. R. Parkin, M. Heeney, L. McCulloch, T. D. Anthopoulos, J. E. Anthony, O. D. Jurchescu, *Adv. Mater.* 2013, **25**, 4352. (b) J. Zhou, Y. Zuo, X. J. Wan, G. K. Long, Q. Zhang, W. Ni, Y. S. Liu, Z. Li, G. R. He, C. X. Li, B. Kan, M. M. Li, Y. S. Chen, *J. Am. Chem. Soc.* 2013, **135**, 8484. (c) M. M. Torrent, C. Rovira, *Chem. Soc. Rev.* 2008, **37**, 827. (d) K. Y. Chi, H. W. Hsu, S. H. Tung, C. L. Liu, *ACS Appl. Mater. Interface.*, 2015, **7**, 5663. (e) J. B. Giguere, N. S. Sariciftci, J. F. Morin, *J. Mater. Chem. C*, 2015, **3**, 601. (f) T. Takahashi, S. Tamura, Y. Akiyama, T. Kadoya, T. Kawamoto, T. Mori, *Appl. Phys. Express.* 2012, **5**, 061601.
- (a) B. R. Baker, R. Y. Lai, M. S. Wood, E. H. Doctor, A. J. Heeger, K. W. Plaxco, *J. Am. Chem. Soc.*, 2006, **128**, 3138. (b) J. M. Zhou, W. Shi, N. Xu, P. Cheng, *Inorg. Chem.* 2013, **52**, 8082. (c) M. H. Zheng, M. M. Zhang, H. H. Li, J. Y. Jin, *J. Fluoresc.*, 2012, **22**, 1421.
- (a) H. Li, Q. F. Xu, N. J. Li, R. Sun, J. F. Ge, J. M. Lu, H. W. Gu and F. Yan, *J. Am. Chem. Soc.*, 2010, **132**, 5542. (b) S. F. Miao, H. Li, Q. F. Xu, N. J. Li, J. W. Zheng, R. Sun, J. M. Lu and C. M. Li, *J. Mater. Chem.*, 2012, **22**, 16582. (c) S. F. Miao, H. Li, Q. F. Xu, Y.

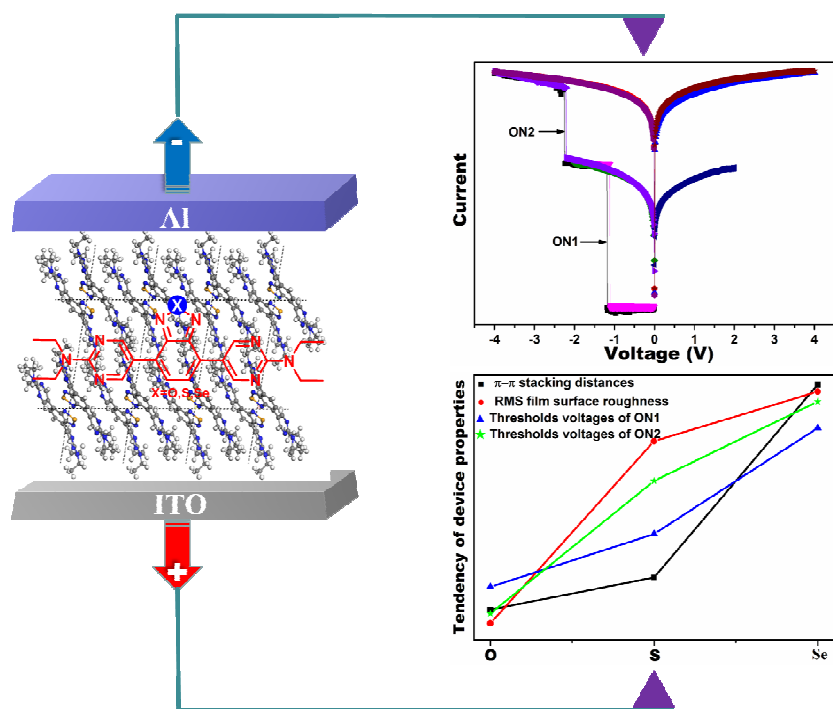
- Y. Li, S. J. Ji, N. J. Li, L. H. Wang, J.W. Zheng and J. M. Lu, *Adv. Mater.*, 2012, **24**, 6210. (d) H. Zhuang, Q. J. Zhang, Y. X. Zhu, X. F. Xu, H. F. Liu, N. J. Li, Q. F. Xu, H. Li, J. M. Lu and L. H. Wang, *J. Mater. Chem. C*, 2013, **1**, 3816. (e) G. Wang, S. F. Miao, Q. J. Zhang, H. F. Liu, H. Li, N. J. Li, Q. F. Xu, J. M. Lu, L. H. Wang, *Chem. Commun.* 2013, **28**, 947. (f) P. Y. Gu, F. Zhou, J. K. Gao, G. Li, C. Y. Wang, Q. F. Xu, Q. C. Zhang, J. M. Lu, *J. Am. Chem. Soc.*, 2013, **135**, 14086. (g) Z. J. Liu, E. B. Shi, Y. Wan, N. J. Li, D. Y. Chen, Q. F. Xu, H. Li, J. M. Lu, K. Q. Zhang, L. H. Wang, *J. Mater. Chem. C*, 2015, **3**, 2033
- 5 (a) Y. L. Shang, Y. Q. Wen, S. L. Li, S. X. Du, X. B. He, L. Cai, Y. F. Li, L. M. Yang, H. J. Gao, Y. L. Song, *J. Am. Chem. Soc.*, 2007, **129**, 11674. (b) C. Q. Ye, Q. Peng, M. Z. Li, J. Luo, Z. M. Tang, J. Pei, J. M. Chen, Z. G. Shuai, L. Jiang and Y. L. Song, *J. Am. Chem. Soc.*, 2012, **134**, 20053; (c) S. J. Liu, P. Wang, Q. Zhao, H. Y. Yang, J. Wong, H. B. Sun, X. C. Dong, W. P. Lin and W. Huang, *Adv. Mater.*, 2012, **24**, 2901. (d) G. Li, K. Zhang, C. Y. Wang, K. S. Leck, F. Z. Hu, X. W. Sun, Q. C. Zhang, *ACS Appl. Mater. Interfaces.*, 2013, **5**, 6458.
- 6 (a) S. Moller, C. Perlov, W. Jackson, C. Taussig, S. R. Forrest, *Nature.*, 2003, **426**, 166. (b) J. C. Scott and L. D. Bozano, *Adv. Mater.*, 2007, **19**, 1452.
- 7 (a) Y. S. Park, T. S. Kale, C.-Y. Nam, D. Choi and R. B. Grubbs., *Chem. Commun.*, 2014, **50**, 7964. (b) G. L. Gibson, D. Gao, A. A. Jahnke, J. Sun, A. J. Tilley, D. S. Seferos, *J. Mater. Chem. A*, 2014, **2**, 14468. (c) B. Nicolas, M. Alexandre, G. David, W. Salem, B. Emily, N. P. Rodica, B. Michel, D. Gilles, T. Ye, L. Mario, *J. Am. Chem. Soc.*, 2008, **130**, 732. (d) J. Soloducho, J. Cabaj, K. Olech, P. Data, M. Lapkowski, *Curr. Org. Chem.*, 2013, **17**, 283.
- 8 (a) A. Yassin, P. Leriche, M. Allain, J. Roncali, *New J. Chem.*, 2013, **37**, 502. (b) J. Zhang, G. L. Wu, C. He, D. Deng, Y. F. Li, *J. Mater. Chem.*, 2011, **21**, 3768. (c) W. Ni, X. Q. Wan, M. M. Li, Y. C. Wang, Y. S. Chen, *Chem. Commun.*, 2015, **51**, 4936.
- 9 (a) P. M. Beaujuge, S. Ellinger, J. R. Reynolds, *Nat. Mater.* 2008, **7**, 795. (b) Q. Peng, K. Park, T. Lin, M. Durstock, L. Dai, *J. Phys. Chem. B.*, 2008, **112**, 2801. (c) P. M. Beaujuge, W. Pisula, H. N. Tsao, S. Ellinger, K. Müllen, J. R. Reynolds, *J. Am. Chem. Soc.* 2009, **131**, 7514.
- 10 (a) W. Elsayy, H. Kang, K. Yu, A. Elbarbary, K. Lee, J. S. Lee, *J. Polym. Sci., Part A: Polym. Chem.* 2014, **52**, 2926. (b) B. A. Coombs, B. D. Lindner, R. M. Edkins, F. Rominger, A. Beeby, U. H. F. Bunz, *New J. Chem.*, 2012, **36**, 550. (c) S. Q. Zhang, L. Ye, W. C. Zhao, D. L. Liu, H. F. Yao, J. H. Hou, *Macromolecules*, 2014, **47**, 4653.
- 11 (a) G. L. Gibson, T. M. McCormick, D. S. Seferos, *J. Am. Chem. Soc.*, 2012, **134**, 539. (b) P. Elena, Z. Natalia, P. Asit, R. Yonatan, B. Michael, *J. Am. Chem. Soc.*, 2014, **136**, 5138. (c) P. B. Pati, S. P. Senanayak, K. S. Narayan, S. S. Zade, *ACS Appl. Mater. Interfaces.*, 2013, **5**, 12460. (d) S. Das, P. B. Pati, S. S. Zade, *Macromolecules*, 2012, **45**, 5410.
- 12 (a) M. Zhang, H. N. Tsao, W. Pisula, C. Yang, A. K. Mishra, K. Mullen, *J. Am. Chem. Soc.* 2007, **129**, 3472–3473. (b) J. K. Lee, M. C. Gwinner, R. Berger, C. Newby, R. Zentel, R. H. Friend, H. Sirringhaus, C. K. Ober, *J. Am. Chem. Soc.* 2011, **133**, 9949. (c) Y. Lin, H. Fan, Y. Li, X. Zhan, *Adv. Mater.* 2012, **24**, 3087.
- 13 (a) D. S. Chung, H. Kong, W. M. Yun, H. Cha, H.K. Shim,; Y.H. Kim, C. E. Park, *Org. Electron.*, 2010, **11**, 899. (b) S. Das,; S. S. Zade, *Chem. Commun.*, 2010, **46**, 1168. (c) S. Haid, A. Mishra, C. Urich, M. Pfeiffer, P. Bauerle, *Chem. Mater.*, 2011, **23**, 4435.
- 14 (a) J. M. Jiang, P. A. Yang, H. C. Chen, K. H. Wei, *Chem. Commun.*, 2011, **47**, 8877. (b) P. Ding, C. Zhong, Y. Zou, C. Pan, Wu, H.; Cao, Y. *J. Phys. Chem. C.*, 2011, **115**, 16211. (c) J. M. Jiang, P. Raghunath, H. K. Lin, Y. C. Lin, M. C. Lin, K. H. Wei, *Macromolecules.*, 2014, **47**, 7070.
- 15 (a) B. Zhang, X. Hu, M. Wang, H. Xiao, X. Gong, W. Yang, Y. Cao, *New J. Chem.*, 2012, **36**, 2042. (b) Z.G. Zhang, J. Wang, *J. Mater. Chem.*, 2012, **22**, 4178. (c) M. C. Scharber, D. Muhlbacher, M. Koppe, P. Denk, C. Waldauf, A. J. Heeger, C. J. Brabec, *Adv. Mater.*, 2006, **18**, 789.
- 16 (a) A. Patra, Y. H. Wijsboom, S. S. Zade, M. Li, Y. Sheynin, G. Leitus, M. Bendikov, *J. Am. Chem. Soc.* 2008, **130**, 6734. (b) J. Hou, M. H. Park, S. Zhang, Y. Yao, L. M. Chen, J. H. Li, Y. Yang, *Macromolecules.*, 2008, **41**, 6012.
- 17 (a) J. H. Hou, T. L. Chen, S. Q. Zhang, H. Y. Chen, Y. Yang, *J. Phys. Chem. C.*, 2009, **113**, 1601. (b) J. H. Kim, J. B. Park, S. A. Shin, M. H. Hyun, D. H. Hwang, *Polymer.*, 2014, **55**, 3605. (c) A. Cihaner, F. Algi, *Adv. Funct. Mater.*, 2008, **18**, 3583.
- 18 (a) J. Warnan, A. E. Labban, C. Cabanetos, E. T. Hoke, P. K. Shukla, C. Risko, J. L. Bredas, M. D. McGehee, P. M. Beaujuge, *Chem. Mater.* 2014, **26**, 2299. (b) H. W. Lin, W. Y. Lee,; C. Lu, C. J. Lin, H. C. Wu, Y. W. Lin, B. Ahn, Y. Rho, M. Ree, W. C. Chen, *Polym. Chem.*, 2012, **3**, 767. (c) W. H. Lee, S. K. Son, K. Kim,; S. K. Lee, W. S. Shin, S. J. Moon, I. N. Kang, *Macromolecules.*, 2012, **45**, 1303.
- 19 (a) A. Yassin, P. Leriche, M. Allain, J. Roncali, *New J. Chem.*, 2013, **37**, 502. (b) J. Zhang, G. L. Wu, C. He, D. Deng, Y. F. Li, *J. Mater. Chem.*, 2011, **21**, 3768. (c) W. Ni, X. Q. Wan, M. M. Li, Y. C. Wang, Y. S. Chen, *Chem. Commun.*, 2015, **51**, 4936.
- 20 (a) W.-Y. Lee, T. Kurosawa, S.-T. Lin, T. Higashihara, M. Ueda, W.-C. Chen, *Chem. Mater.*, 2011, **23**, 4487. (b) M. Hagiri, N. Ichinose, C. Zhao, H. Horiuchi, H. Hirtasuka, T. Nakayama, *Chem. Phys. Lett.*, 2004, **391**, 297.
- 21 J. M. Jiang, P. A. Yang, T. H. Hsieh, K. H. Wei, *Macromolecules* 2011, **44**, 9155.
- 22 (a) J. Rivnay, S. C. B. Mannsfeld, C. E. Miller, A. Salleo, M. F. Toney, *Chem. Rev.* 2012, **112**, 5488. (b) M. S. Chen, J. R. Niskala, D. A. Unruh, C. K. Chu, O. P. Lee, J. M. J. Frechet, *Chem. Mater.* 2013, **25**, 4088. (c) T. L. Nelson, T. M. Young, J. Y. Liu, S. P. Mishra, J. A. Belot, C. L. Balliet, A. E. Javier, T. Kowalewski, R. D. McCullough, *Adv. Mater.* 2010, **22**, 4617. (d) V. S. Gevaerts, E. M. Herzig, M. Kirkus, K. H. Hendriks, M. M. Wien, J. Perlich, P. M. Buschbaum, R. A. J. Janssen, *Chem. Mater.* 2014, **26**, 916.
- 23 (a) A. Patra, Y. H. Wijsboom, S. S. Zade, M. Li, Y. Sheynin, G. Leitus, M. Bendikov, *J. Am. Chem. Soc.*, 2008, **130**, 6734. (b) J. Hou, T. L. Chen, S. Zhang, H. Y. Chen, Y. Yang, *J. Phys. Chem. C.*, 2009, **113**, 1601. (c) W. Zhao, W. Cai, R. Xu, W. Yang, X. Gong, H. Wu, Y. Cao, *Polymer.*, 2010, **51**, 3196.

Effect of single atom substitution in Benzochalcogendiazole Acceptors on the performance of ternary Memory Devices

Zhaojun Liu, Jinghui He, Hao Zhuang, Hua Li,* Najun Li, Dongyun Chen, Qingfeng

Xu, Keqin Zhang, Jianmei Lu,* and Lihua Wang,

Table of Contents



Novelty: Ternary memory storage performances of three Benzooxadiazole-derivatives based devices clearly demonstrate the effect of a single atom substitution from oxygen to sulfur, selenium on the molecular planarity, π - π stacking, film morphologies and device threshold voltages.